Supporting information for

How tobacco (*Nicotiana tabacum*) BY-2 cells cope with Eu(III) – A microspectroscopic study.

Max Klotzsche,[a] Manja Vogel,[b] Susanne Sachs,[a] Johannes Raff,[a] Thorsten Stumpf,[a] Björn Drobot,[a] Robin Steudtner,[a*]

[a] Helmholtz-Zentrum Dresden-Rossendorf e.V., Insitute of Resource Ecology, Bautzner Landstraße 400, 01328 Dresden, Germany

[b] VKTA – Strahlenschutz, Analytik & Entsorgung Rossendorf e.V., Bautzner Landstraße 400, 01328 Dresden, Germany

*correspondence: r.steudtner@hzdr.de

Principal Eu(III) luminescence spectra

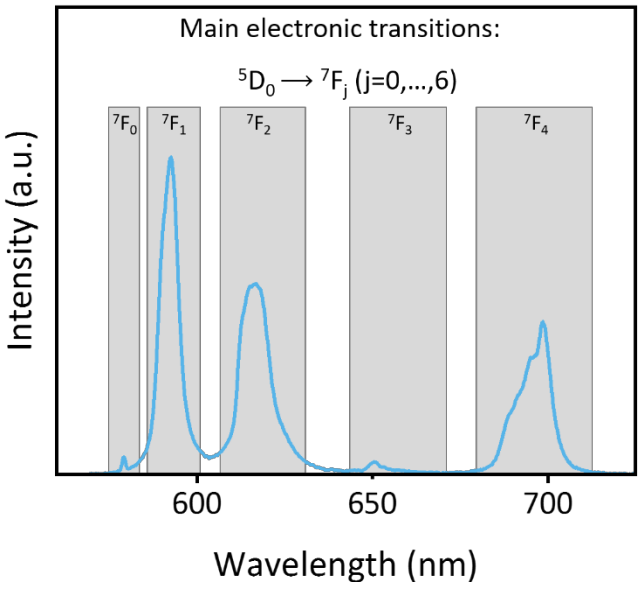

Fig. S 1: Example of an emission spectrum of Eu(III). Luminescence emission mainly originates from the $^5D_0$ excited state to the J levels of the ground term ^7F_j with j=0,…6. Often the transitions to the $^7F_5$ and $^7F_6$ levels are not observed and hence not shown in here. ^7F_j level can split due to the crystal-field effect into 2j+1 sub-levels, depending on the symmetry of the crystal field. Therefore, unsymmetrical shapes of individual emission bands are observed and enable the interpretation of luminescence spectra.

Eu(III) species in the liquid medium

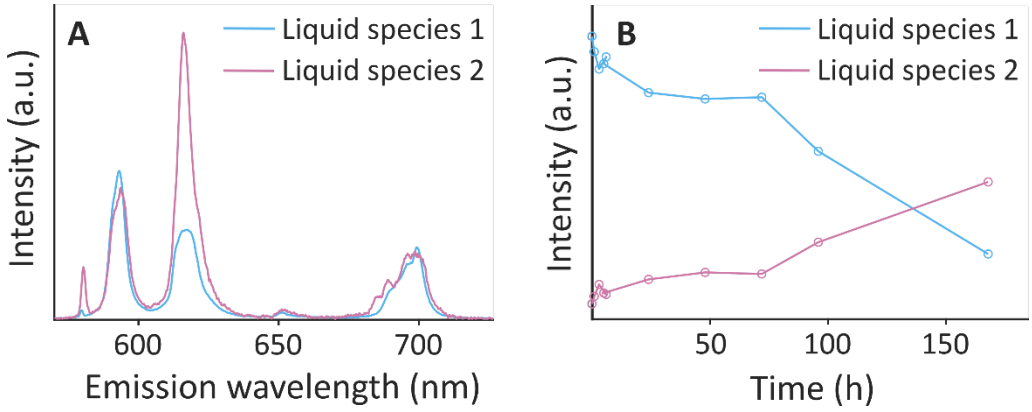

Fig. S 2: Deconvolution results from TRLFS data of the time-dependent incubation of BY-2 cells with 100 µM Eu(III), derived from PARAFAC. **A** Normalized single component spectra of Eu(III) species present in the supernatant after separation from the cell pellet, **B** Species distribution in dependence on exposure time. Liquid species 1 represents the bioavailable Eu(III)-aquo ion which dominates Eu(III) luminescence in the supernatant throughout the first 96 h of exposure. The proportion of liquid species 2 increases with time. Considering the medium composition, a Eu(III)-EDTA species can be suspected herein, which is probably a less bioavailable form of Eu(III).

PARAFAC results from TRLFS data of cell pellets

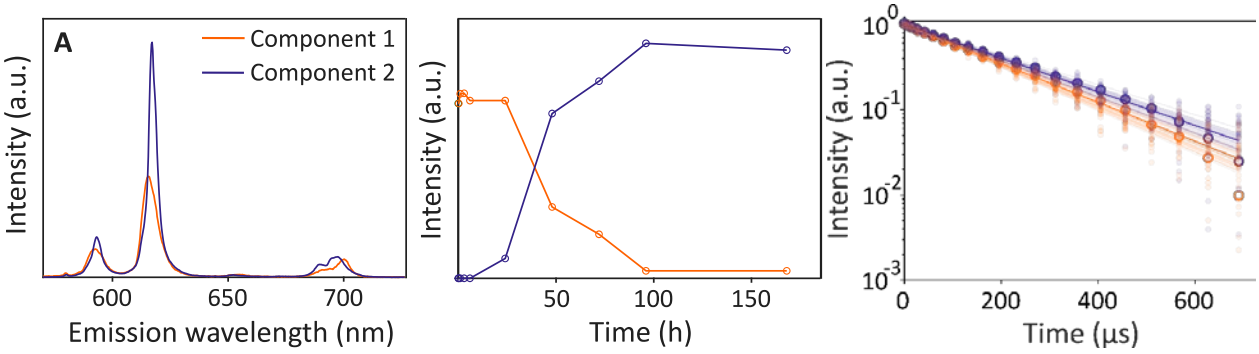

Fig. S 3: Deconvolution results from TRLFS data of cell pellets exposed to 100 µM Eu(III), derived from PARAFAC. **A** Normalized single component spectra of Eu(III) species present in the cell pellets, **B** Component distribution in dependence on exposure time. **C** Luminescence decay fit of both components. Component 1 exhibits a luminescence lifetime of τ_1=190 µs and component 2 of τ_2=219 µs.

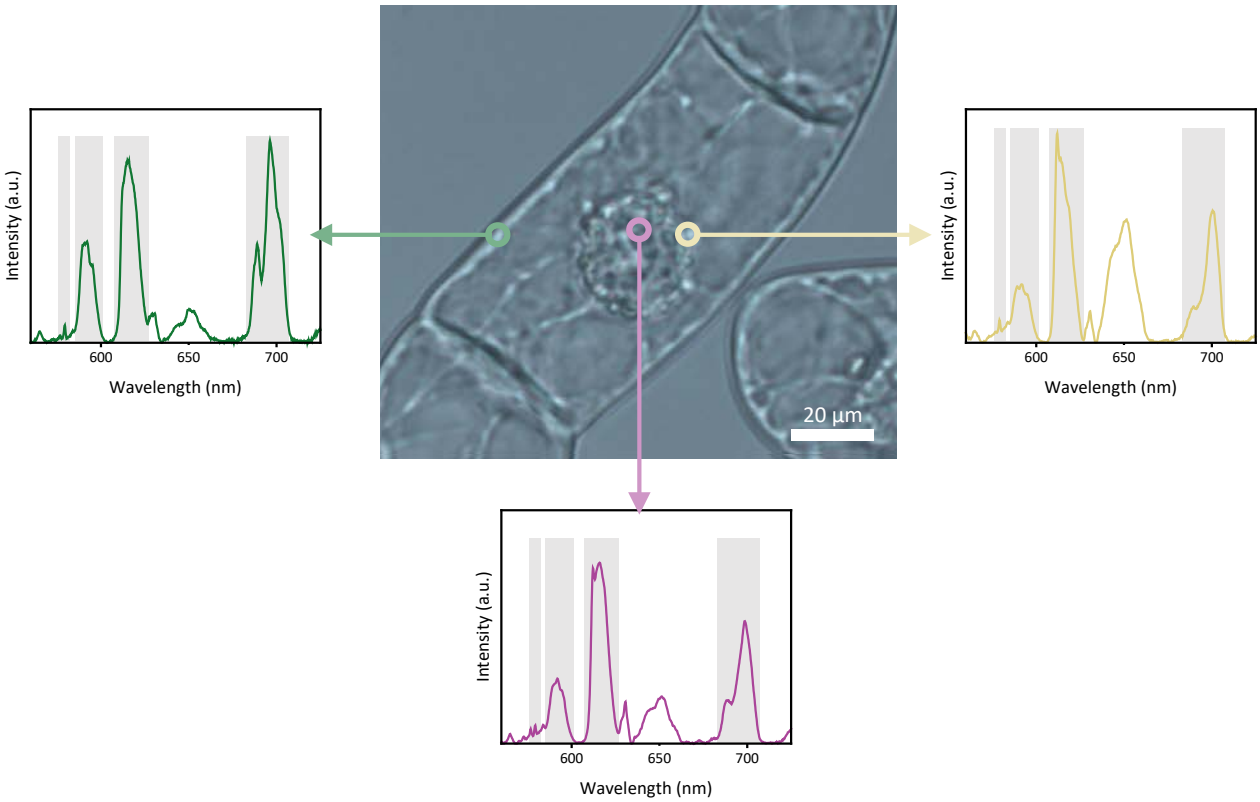

Fig. S 4: Raw spectra acquired at different cellular compartments of tobacco BY-2 cells exposed to 100 µM Eu(III) for 24 h. Excitation with 532 nm gives rise to both, Eu(III) luminescence (highlighted in grey) and Raman bands, most remarkably the H–O stretching mode of water at ≈650 nm. Eu(III) spectra vary in band ratios and band shape due to different coordination of the Eu(III) ion within the cell. For instance, the yellow spectrum resembles phosphatic Eu(III) spectra, whereas the green spectrum likely corresponds to Eu(III)–carboxylate binding environments.

Distribution maps of single Eu(III) luminescence species, derived from deconvolution with NIFA.

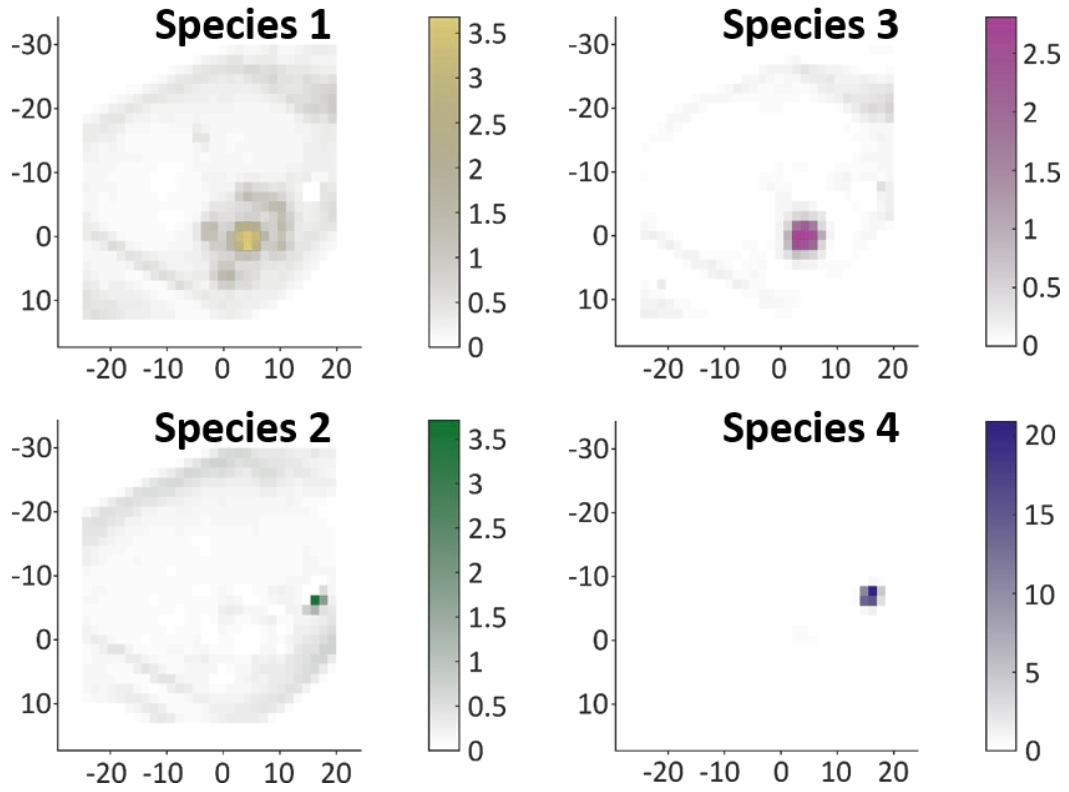

Fig. S 5: Distribution maps for single species of Eu(III) in tobacco BY-2 cells, derived from NIFA. Species 1 corresponds to Eu(III) coordinated to organic phosphate groups, *e.g.* of DNA or RNA. Species 2 likely results from a carboxylate and hydroxyl binding motif. Species 3, with particular occurrence in the nucleolus, is denoted to a protein-bound Eu(III), whereas species 4 is located at the position of the Eu(III)-containing oxalate biomineral.

Eu(III)-containing oxalate biominerals in tobacco BY-2 cells

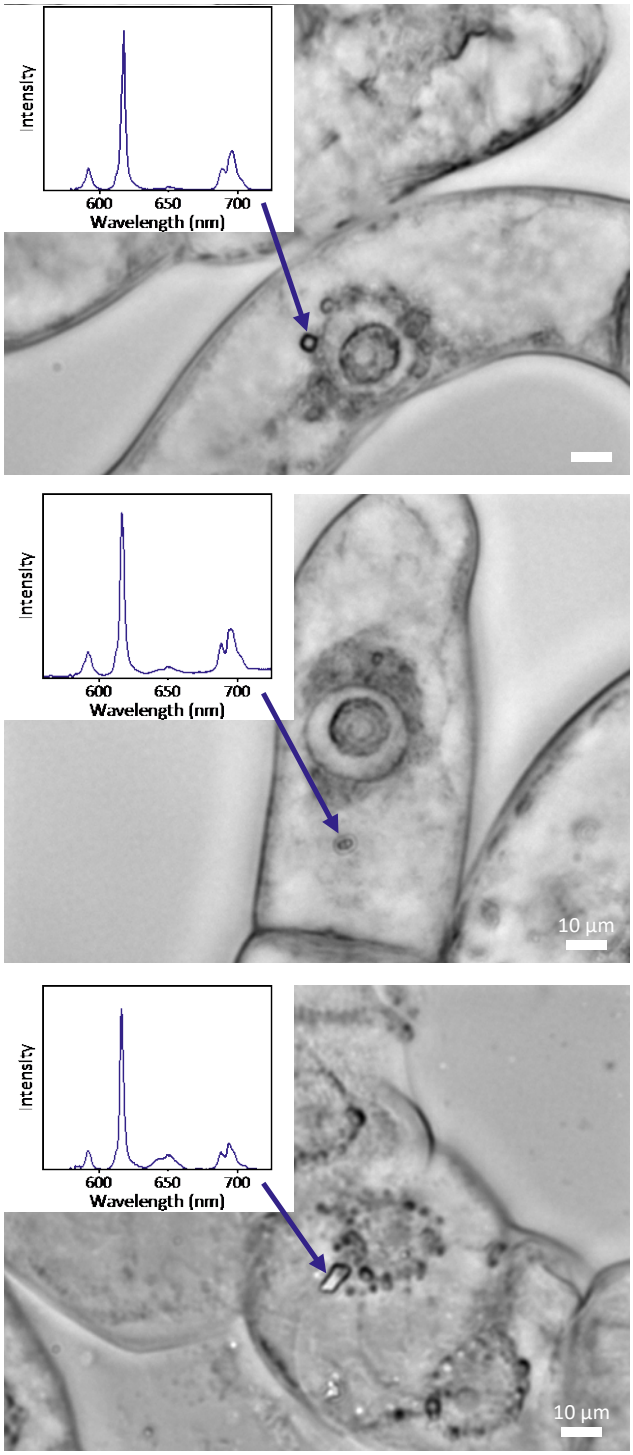

Fig. S 6: Differential interference contrast microscopy (DIC) images of tobacco BY-2 cells incubated with 100 µM Eu(III) for 48 h and spectra acquired with 532 nm excitation wavelength. Each cell contains one oxalate biomineral that, according to the respective spectrum, comprises of Eu(III). Different morphologies can be seen herein, *e.g.* rectangular, circular and rhomboid. Spectra shown here are not deconvoluted, *i.e.* they comprise of luminescence and Raman bands.

Correlative microscopic and spectroscopic examination of tobacco BY-2 cells subsequent to Ln exposure and control cells without Ln affliction

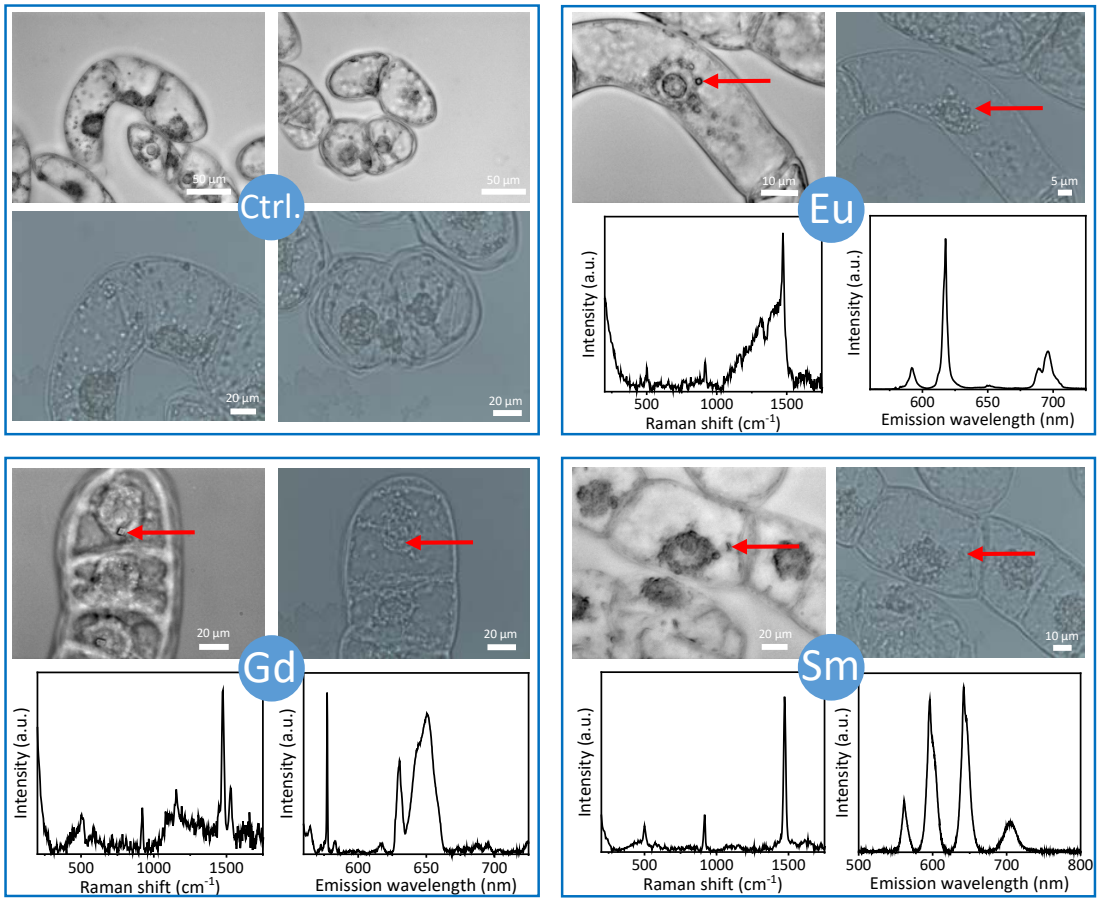

Fig. S 7: Correlative allocation of Ln oxalate crystals in tobacco BY-2 cells by differential interference contrast microscopy and chemical microscopy with respective Raman and luminescence spectra. For control cells (without Ln), no Raman oxalate signals could be recorded. Bioprecipitates in Eu-, Gd- and Sm-incubated cells show characteristic oxalate Raman signals upon excitation with 633 nm. Additionally, those bioprecipitates in Eu- and Sm-incubated cells exhibit luminescence bands upon excitation with 532 nm and 473 nm, respectively, whereas Gd precipitates only give rise to a Raman water band.

Reference emission spectra of some Eu(III)-compounds measured by TRLFS

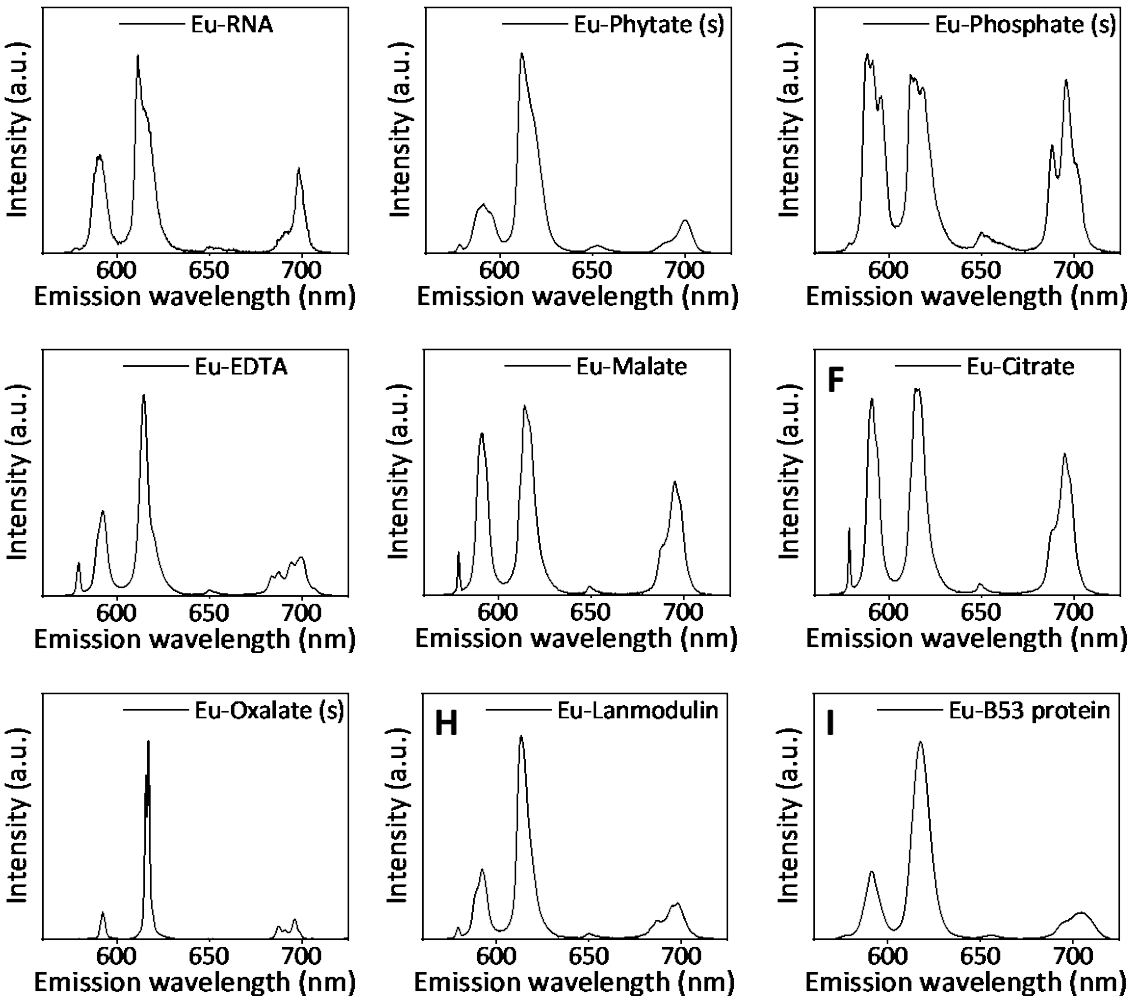

Fig. S 8: Reference spectra of Eu(III) compounds. **A** Emission spectrum of Eu(III) coordinated by functional groups, *e.g.* phosphate groups, of RNA from torula yeast Type VI, [Eu(III)]=10 µM, [RNA]=76 µM,[1] **B** Emission spectrum of powdered Eu(III)-phytate, **C** Emission spectrum of powdered Eu(III)-phosphate, **D** Emission spectrum of Eu(III)-EDTA, [Eu(III)]=10 µM, [EDTA]=40 µM, **E** Emission spectrum of Eu(III)-malate, [Eu]=10 µM, [Malate]=76 µM, **F** Emission spectrum of Eu(III)-citrate, [Eu]=10 µM, [Citrate]=76 µM, **G** Emission spectrum of powdered Eu(III)-oxalate decahydrate, synthesized according to Alexander *et al.*,[2] **H** Emission spectrum of Eu(III) coordinated with the active site of the peptide Lanmodulin,[3] **I** Emission spectrum of Eu(III) coordinated with the active site of S-layer protein B53.. **A, B, C** represent examples of phosphatic binding motif, whereas **D, E, F, G** show Eu(III)-compounds that involve carboxylic groups in their coordination. **H** and **I** represent proteinaceous Eu(III) coordination.

References

1 M. Vogel, R. Steudtner, T. Fankhänel, J. Raff and B. Drobot, *Analyst*, 2021, **146**, 6741–6745.

2 D. Alexander, K. Thomas, M. Joy, P. R. Biju, N. V. Unnikrishnan and C. Joseph, *Acta Crystallogr C Struct Chem*, 2019, **75**, 589–597.

3 S. M. Gutenthaler, S. Tsushima, R. Steudtner, M. Gailer, A. Hoffmann-Röder, B. Drobot and L. J. Daumann, *Inorg Chem Front*, 2022, **9**, 4009–4021.